

# We are IntechOpen, the world's leading publisher of Open Access books Built by scientists, for scientists

4,400

Open access books available

117,000

International authors and editors

130M

Downloads

Our authors are among the

154

Countries delivered to

TOP 1%

most cited scientists

12.2%

Contributors from top 500 universities



WEB OF SCIENCE™

Selection of our books indexed in the Book Citation Index  
in Web of Science™ Core Collection (BKCI)

Interested in publishing with us?  
Contact [book.department@intechopen.com](mailto:book.department@intechopen.com)

Numbers displayed above are based on latest data collected.  
For more information visit [www.intechopen.com](http://www.intechopen.com)



---

# Dielectric Materials for Compact Dielectric Resonator Antenna Applications

---

L. Huitema and T. Monediere

Additional information is available at the end of the chapter

<http://dx.doi.org/10.5772/50612>

---

## 1. Introduction

Dielectric resonators using high-permittivity materials were originally developed for microwave circuits, such as filters or oscillators as tuning element [1]. Indeed, in the late nineteen sixties, the development of low-loss ceramic materials opened the way for their use as high-Q elements [2-4]. Then, making use of dielectric materials to create the dielectric resonator antenna (DRA) illustrates the ingenuity of Professor S. A. Long [5], who was the first to propose such a procedure in the early nineteen eighties. Indeed, it introduced the use of a dielectric resonator as an antenna by exciting different modes using multiple feeding mechanisms. During the nineties, emphasis was placed on applying analytical or numerical techniques for determining input impedance, fields inside the resonator and Q-factor [6]. Kishk, Junker, Glisson, Luk, Leung, Mongia, Bhartia, Petosa and so on, have described a significant amount of DRAs' analyses and characterizations [7-18]. Petosa and al. proposed both in literatures and book [6,12] many of the recent advances on DRAs.

Current DRA literatures focus on compact designs to address portable wireless applications. Among them, new DRA shapes or hybrid antennas are developed to enhance the antenna impedance bandwidth [13-19] or for multiband antenna applications [20-22].

The first part will address a brief overview of the most common used DRA shapes and structures including both rectangular and cylindrical DRAs. The emphasis will be placed on better understanding what DRAs exactly are and how to develop such an antenna. This part will detail fundamental modes of DRAs, their resonant frequencies, fields inside the resonator and radiation patterns corresponding to these modes.

A second part will focus on the relevant dielectric material properties having a significant contribution to achieve better antenna performances. It will detail the kind of materials DRAs can use, which is closely linked to the targeted application.

Multiple techniques to miniaturize such an antenna will be presented in the third part, supported by concrete examples. At the same time, everyone will be able to appreciate that dielectric material properties have a major role to play in designing a DRA. It should be noted that the material choice is even more critical when the targeted challenge is the antenna size reduction.

Therefore, depending on the intended applications, this part will enable to find the best trade-off between the material choice and its shape.

Although some wideband or multiband DRA structures have been introduced in the third part, the fourth and last part will be dedicated to a new method to design a DRA. It will address engineering design data on hybrid modes creation to enhance the bandwidth or develop multiband antennas. This part will include many references to clearly explain this research method while highlighting their contribution to expand the use of DRA in new kind of mobile handheld devices (e.g. new tablets).

## 2. Overview on DRA studies

The design of a DRA in any geometry must satisfy various specifications including: the resonant frequency, the impedance bandwidth, the field distribution inside the resonator and also the radiated field. The intent of this part is to provide an understanding of fundamental operation of DRAs, emphasizing both design and implementation. Thus, to provide comprehensive research method, this part will start by presenting main findings of investigations on simple-shaped DRAs. Then, it will deal with the different DRA feeding methods. Finally, this part will focus on the study of two DRA shapes: cylindrical and rectangular.

### 2.1. Main DRAs characteristics

A non-exhaustive list of main simple-shaped DRAs characteristics is described below:

- The main dimension of a DRA is proportional to  $\lambda_0 / \sqrt{\epsilon_r \cdot \mu_r}$  where  $\lambda_0$  is the free-space wavelength at the resonant frequency,  $\epsilon_r$  and  $\mu_r$  are respectively the dielectric and the magnetic constant of the material. In a dielectric material case,  $\mu_r = 1$  and the main dimension of a DRA is proportional to  $\lambda_0 / \sqrt{\epsilon_r}$ .
- The radiation efficiency of the DRA is highly depending on the material losses. In case of a low-loss dielectric material, DRAs allow to achieve better efficiency than other kind of antennas because of minimal conductor losses associated with a DRA.
- For a given dielectric constant, both resonant frequency and radiated Q-factor are defined according to the resonator dimensions. That allows having a great flexibility and some degrees of freedom to design such an antenna.
- Another degree of freedom is the large spectrum of available dielectric materials. That allows doing the best trade-off between dimensions and impedance bandwidth according to the intended application.

- A number of modes can be excited within the DRA, many of them provide dipolar-like radiation characteristics.
- The most common targeted frequencies presented by the research literatures are ranging from 1GHz to 40 GHz.
- For a given DRA geometry, the radiation patterns can be made to change by exciting different resonant modes.
- A large number of DRA excitations are currently used, e.g. microstrip line, coaxial probe excitation, coplanar waveguide... The next subsection will deal with the most commonly used excitations.

## 2.2. Common DRAs feedings

Multiple feeding mechanisms are employed to excite different resonator modes. This subsection will summarise most widely-used excitations while giving many references in order designers to choose the most appropriate excitation.

### 2.2.1. Coaxial probe excitation

It can be located within the DRA or adjacent to it. Within the DRA, a good coupling can be achieved by aligning the probe along the electric field of the DRA mode as shown Figure 1.

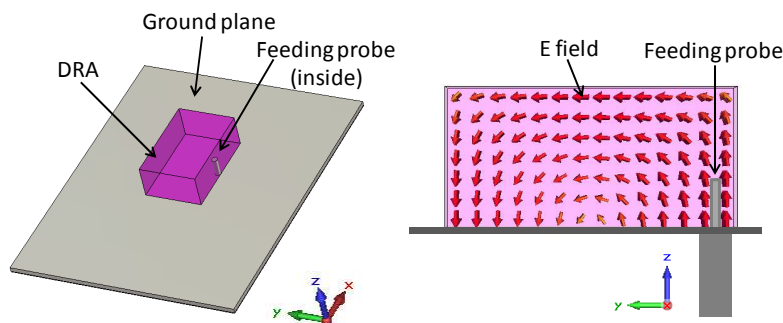


**Figure 1.** Coaxial probe coupling the E field

The adjacent position is currently used to couple the magnetic field of the DRA mode (Figure 2). In these both cases, the probe is exciting the  $TE_{111}$  fundamental mode of the rectangular DRA.

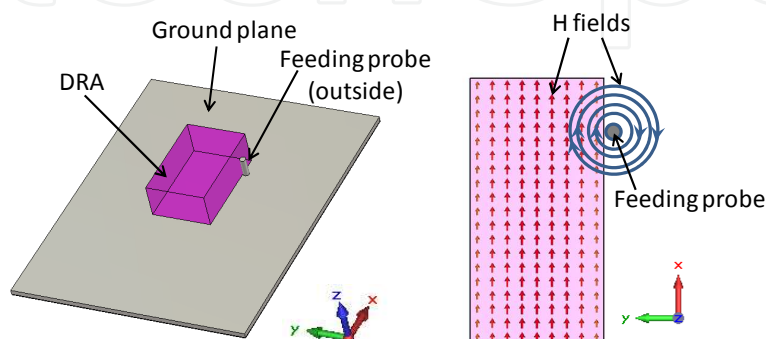


**Figure 2.** Coaxial probe coupling the H field

When the excitation probe is inside the resonator, particular attention has to be paid to the air gap between the probe excitation and the dielectric material. Indeed, an air gap results in a lower effective dielectric constant, which entails both a decrease in the Q-factor and a shift of the resonance frequencies [23-24]. The probe location allows choosing the intended excited mode and the coupling of the mode can be optimized by adjusting both length and height of the probe.

### 2.2.2. Microstrip feeding line and coplanar waveguide

The principle is similar to the probe excitation case. A microstrip line placed close to the DRA can couple the magnetic field of the DRA mode. However, this latter can affect the antenna polarisation and can thus increase the parasitic radiation. This could be reduced by placing the line under the resonator as shown Figure 3.

Another way is to replace the microstrip line by a coplanar waveguide, the Figure 3 is presenting a rectangular DRA excited by a coplanar waveguide.

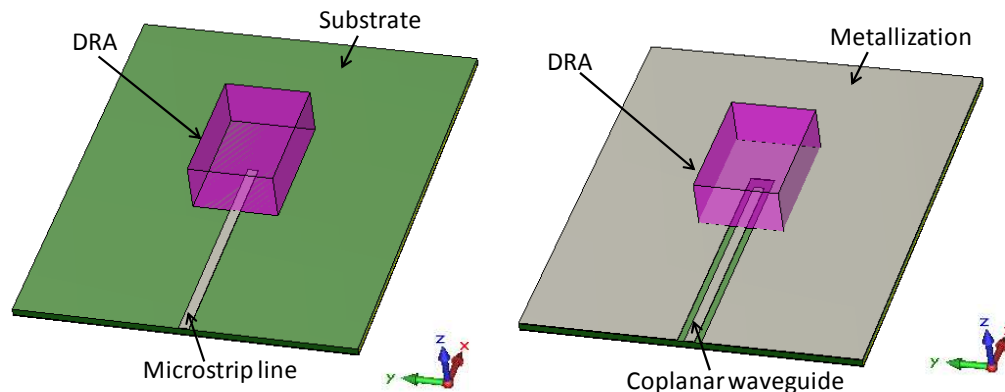


**Figure 3.** Microstrip feeding line and coplanar waveguide

In these both cases, the mode coupling can be optimized by changing the resonator position and/or its dielectric permittivity. For low dielectric permittivity materials (which allows obtaining a wide bandwidth), it is somewhat difficult to excite the mode. There are different solutions to obtain both miniaturization and good coupling, they will be explained in this chapter.

An important point is that these excitation methods are disturbing DRA modes by introducing electrical boundary conditions. This issue is all the more sensitive since the antenna is miniature. The last part of the chapter will show how to take advantage of this issue.

### 2.2.3. Aperture coupling

A common method of exciting a DRA is acting through an aperture in the ground plane. The Figure 4 shows an example of the excitation of the  $TE_{111}$  mode of a rectangular DRA with a rectangular slot. To achieve relevant coupling, the aperture has to be placed in a DRA

strong magnetic area. Feeding the aperture with a microstrip line is a current approach [25-26].

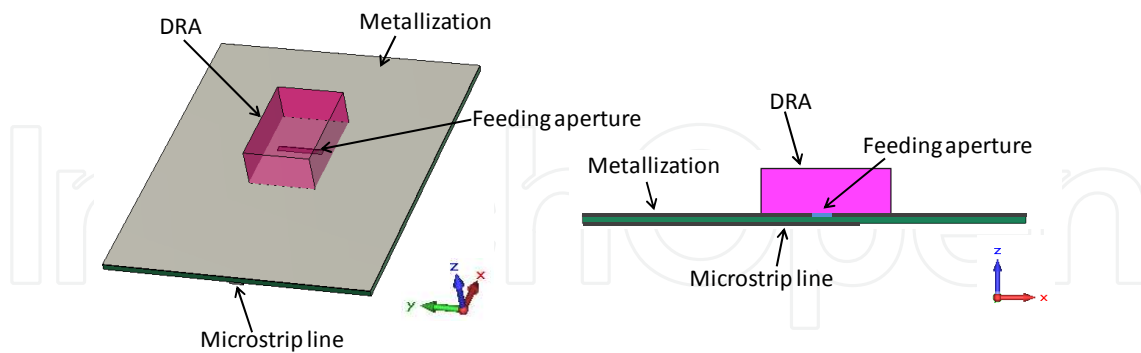


**Figure 4.** Aperture coupling the  $TE_{111}$  mode of the rectangular DRA

The main dimension of the aperture needs to be around  $\lambda_g/2$ , which is highly problematic at low frequencies.

On top of these multiple feeding methods, the choice of different DRAs shapes represents another degree of flexibility and versatility. The next subsection will deal with the cylindrical shape.

### 2.3. The cylindrical DRA

It offers great design flexibility, where both resonant frequency and Q-factor are depending on the ratio of radius/height. Various modes can be excited within the DRA and a significant amount of literature is devoted to their field configurations, resonant frequencies and radiation properties [27-28]. This part will present a complete and concrete study of a cylindrical DRA.

Like most realistic cases, the cylindrical DRA presented Figure 5, is mounted on a finite ground plane. Because dielectric material properties will be studied in very great depth in the third part, the dielectric permittivity  $\epsilon_r$  of the DRA is fixed and chosen equal to 30. It is also characterized by its height  $d$  and its radius  $a$ . To keep the chapter concise while remaining comprehensive, only relevant results and equations will be given.

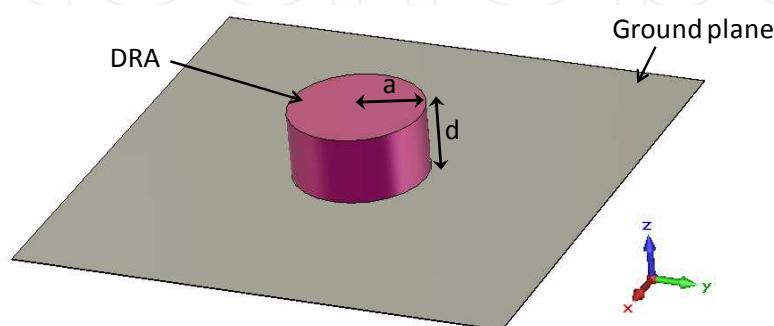


**Figure 5.** Cylindrical DRA

First of all, the study can begin with a modal analysis. This allows determining the most appropriate excitation method. Modes of cylindrical DRA can be divided into three types: TE, TM and hybrid modes, i.e. EH or HE [9-10,30]. The latter have a dependence on azimuth  $\phi$ , while TE and TM modes have no dependence on azimuth. To identify fields' variations according  $\phi$  (azimuth),  $r$  (radial) and  $z$  (axial) directions, subscripts respectively noticed  $n$ ,  $p$  and  $m$  are following the mode notation. Because TE and TM modes have no azimuthal variation,  $n=0$  for these modes. Finally, all cylindrical DRA modes can be defined such as:  $TE_{0pm+\delta}$ ,  $TM_{0pm+\delta}$ ,  $HE_{n\pm pm+\delta}$  and  $EH_{n\pm pm+\delta}$ . The  $\delta$  value is ranging between 0 and 1, it approaches 1 for high  $\epsilon_r$ . It should be noted that  $n$ ,  $m$  and  $p$  are natural numbers. The modal analysis of a DRA can be deducted either with analytical calculations or thanks to electromagnetic simulators like CST Microwave Studio (CST MS).

### 2.3.1. Modal analysis

- Analytical equations derive from the analytical calculations of a cylindrical dielectric resonator by assuming perfect magnetic and/or electric walls on resonator faces. The perfect magnetic wall boundary condition was demonstrated to be valid for high  $\epsilon_r$  values [30], it remains accurate for lower values as well.

Fields equations inside the DRA, resonant frequencies and Q factor are detailed in [7,9] and [12]. Resonant frequencies of all modes are provided hereafter:

$$\begin{pmatrix} f_{TMn\pm pm} \\ f_{TEn\pm pm} \end{pmatrix} = \frac{c}{2\pi a \sqrt{\epsilon_r \mu_r}} \sqrt{\left(\frac{X'_{np}}{X_{np}}\right)^2 + \left(\frac{(2m+1)\pi \cdot a}{2d}\right)^2} \quad (1)$$

Where  $X_{np}$  and  $X'_{np}$  are Bessel's solutions,  $(n, m, p) \in \mathbb{N}^3$ ,  $a$  and  $d$  are the radius and the height of the dielectric resonator.

In the case presented Figure 5, the fundamental excited mode is the  $HE_{11\delta}$  and its resonant frequency equals:

$$f_{110} = \frac{3.10^8}{2\pi \sqrt{30}} \sqrt{\left(\frac{X'_{11}}{0.04}\right)^2 + \left(\frac{\pi}{2 \times 0.045}\right)^2} = 503.6 \text{ MHz} \quad (2)$$

This method requires the resolution of both Maxwell and propagation equations. It was therefore reserved for simple-shaped DRA.

- The "Eigenmode solver" of CST MS allows viewing 3D fields of each mode and having their resonant frequencies. When considering the studied example and defining perfect magnetic boundary conditions on all DRA walls, except for the DRA bottom where perfect electric boundary condition is considered (due to the ground plane), the software gives 504 MHz for the resonant frequency value of the  $HE_{11\delta}$  mode. It is also possible to see both H and E fields of this mode, they are presented Figure 6. This valuable information allows designer to choose the most appropriate excitation of the considered mode.



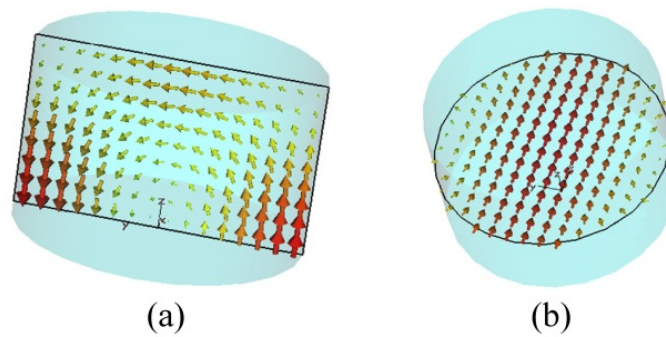


**Figure 6.** E field (a) and H field (b) of the  $HE_{118}$  mode

In light of this above, the best way to excite the  $HE_{118}$  mode is to integrate a coaxial probe along the E field inside the DRA.

Now that the modal analysis was explained and the excitation determined, we can go straight to the electromagnetic study of the DRA.

### 2.3.2. Electromagnetic study

Since input impedance and also  $S_{11}$  parameter cannot be calculated with the magnetic wall model, their study is solely possible with an electromagnetic simulator or of course can be experimentally done. Moreover, electromagnetic simulators facilitate accurate and efficient antenna analysis by providing the complete electric and magnetic fields inside and outside the antenna taking into account the finite ground plane. The impedance, the  $S_{11}$  parameter, the power radiated and the far field radiation pattern are determined everywhere and at any frequency in a single analysis thanks to the Finite Integration Temporal method.

The Figure 7 presents the cylindrical DRA excited by a coaxial probe.

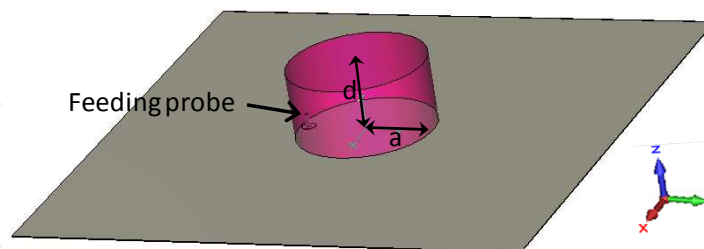


**Figure 7.** Excitation of the  $HE_{118}$  mode with a coaxial probe

Using the CST MS software, the input impedance is presented Figure 8. It shows that the fundamental mode is excited at the resonant frequency fairly corresponding to the predicted value by the modal analysis of 504 MHz. The minor shift between resonant frequencies deduced with modal analysis and electromagnetic study is due to magnetic wall model used during the modal analysis, which is not absolutely accurate.

An important data for antenna designers is the  $S_{11}$  parameter (Figure 8). It is directly deduced from the input impedance parameter.



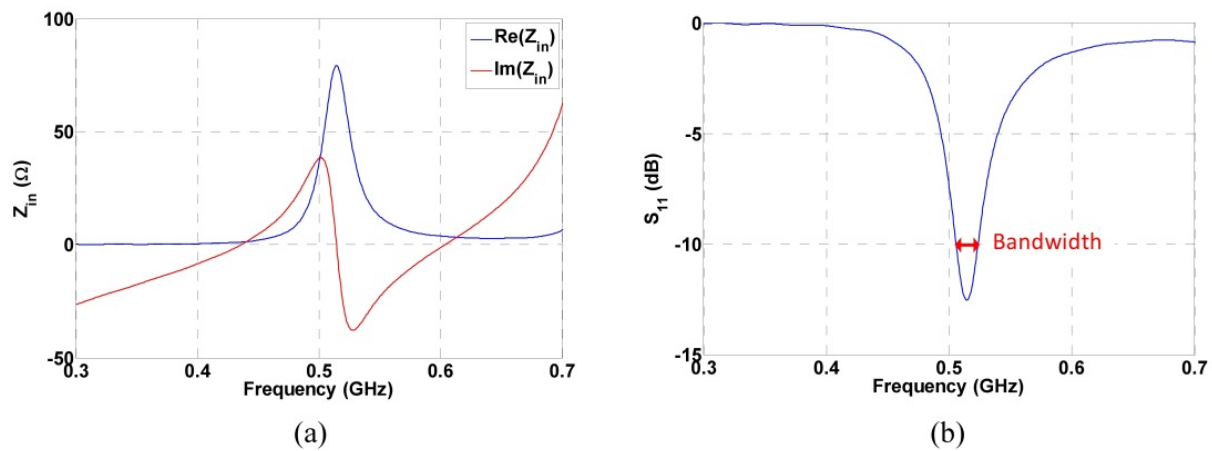


**Figure 8.** Input impedance (a) and  $S_{11}$  parameter (b) of the DRA

It allows knowing the matching frequency as well as the impedance bandwidth, basically corresponding to the working frequencies of the antenna. In this case, the matching frequency equals 510 MHz with 3.6% of bandwidth at -10 dB.

Another important issue is the radiation pattern. It can be expressed in spherical coordinates by using equivalent magnetic surface currents [7]. This can only be done until the DRA is mounted on an infinite ground plane. Using the electromagnetic software is another way of accessing to the 3D radiation pattern. This method is more accurate because it is taking into account the realistic structure (i.e. the finite ground plane). The Figure 9 shows the 3D radiation pattern of the cylindrical DRA using the simulator.

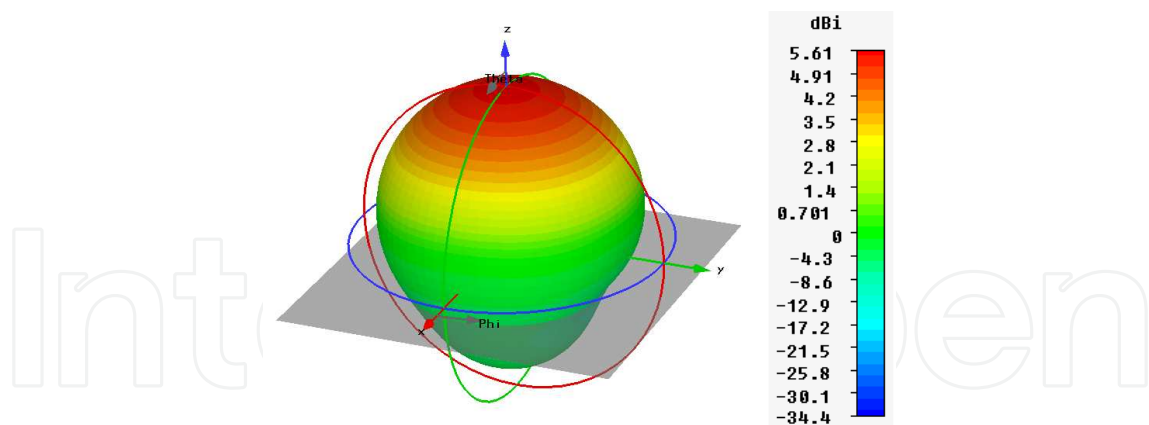


**Figure 9.** 3D radiation pattern

The simulated 3D radiation pattern provides antenna information such as the radiation efficiency, which is defined as the ratio between the radiated to accepted (input) power of the antenna.

The  $HE_{11\delta}$  mode of the cylindrical DRA radiates like a short horizontal magnetic dipole. Concerning other modes, the  $TM_{01\delta}$  radiates like a short electric monopole, while the  $TE_{01\delta}$  mode radiates like a short magnetic monopole.

## 2.4. The rectangular DRA

The rectangular DRA has one degree of freedom more than the cylindrical DRA. Indeed, it is characterized by three independent lengths, i.e. its length  $a$ , its width  $b$  and its height  $d$ . Thus, there is great design flexibility, since the large choice of both dielectric materials and different lengths ratios.

Usually the dielectric waveguide model is used to analyze the rectangular DRA [8-10]. In this approach, the top surface and two sidewalls of the DRA are assumed to be perfect magnetic walls, whereas the two other sidewalls are imperfect magnetic walls. Since the considered case is a realistic one (Figure 10), the DRA is mounted on a ground plane, thus, an electric wall is assumed for the bottom surface.

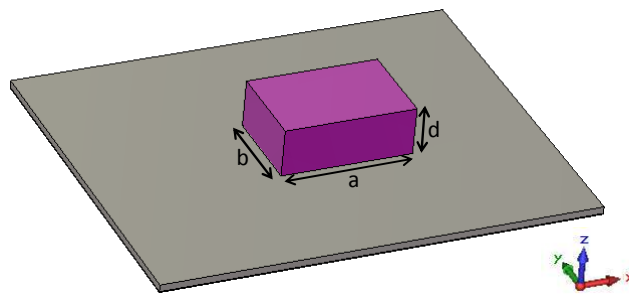


**Figure 10.** Rectangular DRA

The modes in an isolated rectangular dielectric resonator can be divided in two categories: TE and TM modes, but in case of the DRA mounted on a ground plane, only TE modes are typically excited. The fundamental mode is the  $TE_{111}$ . As the three dimensions of the DRA are independent, the TE modes can be along the three directions:  $x$ ,  $y$  and  $z$ . By referring to the Cartesian coordinate system presented Figure 10, if the dimensions of DR are such as  $a > b > d$ , the modes in the order of increasing resonant frequency are  $TE_{z111}$ ,  $TE_{y111}$  and  $TE_{x111}$ . The analysis of all the modes is similar. The example of the  $TE_{z111}$  mode is discussed in [8], the field components inside the resonator and resonant frequencies are analytically presented.

As for the cylindrical case, CST MS can be used to see both  $E$  and  $H$  fields, as presented Figure 11.

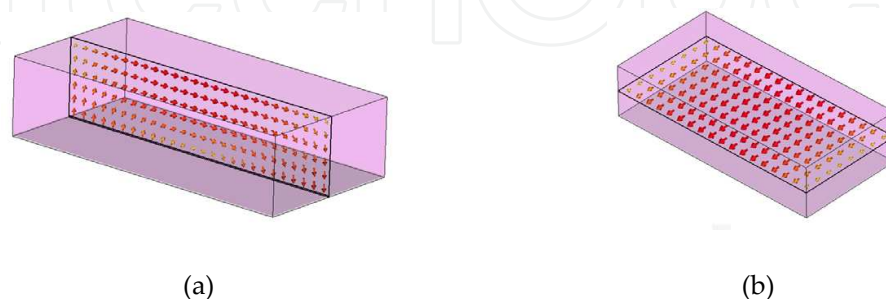


**Figure 11.** E field (a) and H field (b) of the  $TE_{111}$  mode

The resonant frequencies definition is reminded hereafter:

$$f_0 = \frac{c}{2\pi\sqrt{\epsilon_r\mu_r}} \sqrt{k_x^2 + k_y^2 + k_z^2} \quad (3)$$

It is found by solving the following transcendental equation:

$$k_z \tan\left(\frac{k_z a}{2}\right) = \sqrt{(\epsilon_r - 1)k_0^2 - k_z^2} \quad (4)$$

where  $k_x = \frac{\pi}{a}$ ,  $k_y = \frac{\pi}{b}$ ,  $k_0 = \frac{\omega_0}{v} = \frac{2\pi f_0 \sqrt{\epsilon_r \mu_r}}{c}$  and  $k_x^2 + k_y^2 + k_z^2 = k_0^2$

Values of resonant frequencies predicted by using this model are close to the measured ones for moderate to high value of  $\epsilon_r$ . A frequency shift appears for low  $\epsilon_r$  but it remains a good approximation method. If more accuracy is required, the electromagnetic study with CST MS (for example) presented in the cylindrical DRA case will have to be undertaken. Moreover, it allows taking into account feeding mechanism and ground plane dimensions.

Now DRA research method has been initiated, presenting resonant frequencies, fields configuration and feeding mechanisms, the next part will focus on the relevant dielectric material properties having significant influences on antenna performances.

### 3. Analysis on the dielectric material choice

To supply satisfactory answers about the effects of dielectric material properties, this section will present a careful and extensive investigation into relevant cases. Indeed, properties of the dielectric material have an influence on antenna characteristics, i.e. impedance bandwidth, Q factor, resonant frequency and radiation efficiency. Thus, this part will allow the reader to correctly select a dielectric material for a targeted application.

The cylindrical DRA example presented Figure 5 with a radius  $a=40\text{mm}$  and a height  $h=45\text{mm}$  will be pursued here. However, all results included in this part are generally applicable to most shapes of DRAs. A first sub-section will detail the influence of the dielectric permittivity and a second one will be interested in the impact of the dielectric loss tangent on the DRA performances.

Dielectric material properties having an impact on antenna characteristics are dielectric permittivity values and loss tangents.

#### 3.1. Influence of the dielectric permittivity

To show the real impact of dielectric permittivity values, this sub-section will deal with a lossless dielectric material. Analytical studies show that the Q factor of the  $\text{HE}_{11\delta}$  mode is defined as

$$Q = 0.01007 \cdot \epsilon_r \cdot \frac{a}{h} \cdot \left( 1 + 100 \cdot \exp\left(-2.05 \left( \frac{a}{2h} - \frac{1}{80} \left( \frac{a}{h} \right)^2 \right) \right) \right) \quad (5)$$

It is plotted as a function of  $a/h$  for different values of  $\epsilon_r$  in the Figure 12.

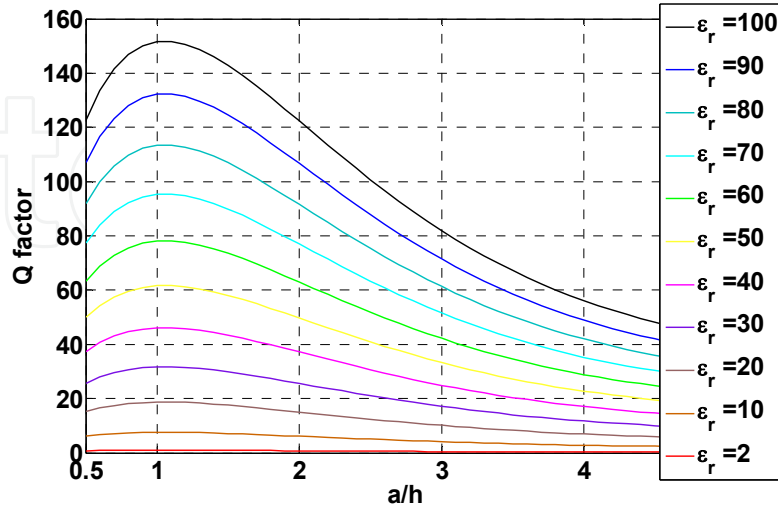


**Figure 12.** Q factor according the  $a/h$  values

Q factor is increasing with  $\epsilon_r$  and reaching a maximum for  $a/h=1.05$ . This Q factor can be used to estimate the fractional bandwidth of an antenna using:

$$BW = \frac{\Delta f}{f_0} = \frac{s-1}{Q\sqrt{s}} \quad (6)$$

Where  $\Delta f$  is the absolute bandwidth,  $f_0$  is the resonant frequency and  $s$  the maximum acceptable voltage standing wave ratio (VSWR).

The Q factor equation is deriving from the cylindrical dielectric resonator model approach by assuming perfect magnetic and/or electric walls on resonator faces. These equations are not absolutely accurate but they offer a good starting point for the design of cylindrical DRAs.

Let's consider the electromagnetic study presented in the first section with the cylindrical DRA example (Figure 7). Previously, the dielectric permittivity was fixed and equaled 30, it is now a variable. The Figure 13 plots both resonant frequencies and impedance bandwidths according to the dielectric permittivity  $\epsilon_r$ . Because the coupling of the mode is depending on both length and height of the probe, this latter has been optimized for each  $\epsilon_r$  value. The Figure 13 is thus the result of a large number of simulations.

As expected (see equation 3), the resonant frequency decreases when the dielectric permittivity increases. Moreover, this Figure shows that the bandwidth is the widest for  $\epsilon_r=10$ . Fields are less confined for a low dielectric permittivity DRA, it is thus more difficult to couple the mode inside the resonator. Indeed, for higher dielectric values ( $\epsilon_r>10$ ), strong coupling is achieved, however, the maximum amount of coupling is significantly reduced if the dielectric permittivity of the DRA is lowered. That is why the bandwidth is low for  $\epsilon_r$

under 10. For a dielectric permittivity over 10, the Q factor is increasing and therefore the impedance bandwidth is decreasing (see equation 5).

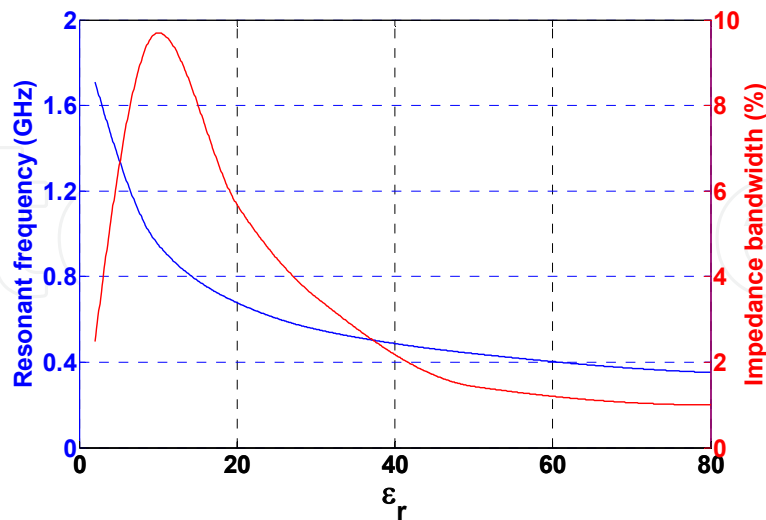


**Figure 13.** Resonant frequency according the dielectric permittivity values  $\epsilon^r$

Now that the influence of the dielectric permittivity has been shown, we can consider in the next sub-section more realistic cases by studying the impact of losses on the antenna characteristics.

### 3.2. Influence of dielectric material losses

Dielectric material losses directly impact the impedance bandwidth and antenna radiation efficiency. Their influence depends on the dielectric permittivity of the material.

Because analytical considerations do not take into account losses, only electromagnetic approaches are available to complete this study. To be more readable and relevant, charts will be provided to present and take into account all effects of losses.

The chosen example is still the same: the cylindrical DRA mounted on a ground plane with a radius and a height respectively equal to 40 mm and 45 mm and excited on its fundamental mode. The study of losses is done for different dielectric permittivity values.

The impedance bandwidth is studied as a first step. The Figure 14 presents the impedance bandwidth according to both dielectric permittivity and tangent loss of the dielectric material.

Several information have to be noted:

The most important loss tangents are, the widest the impedance bandwidth is.

The impedance bandwidth is the widest when for  $\epsilon_r=10$ , whatever the losses.

The radiation efficiency is now investigated. Same simulations are done and the Figure 15 presents the antenna radiation efficiency according to both dielectric permittivity and tangent loss of the dielectric material.

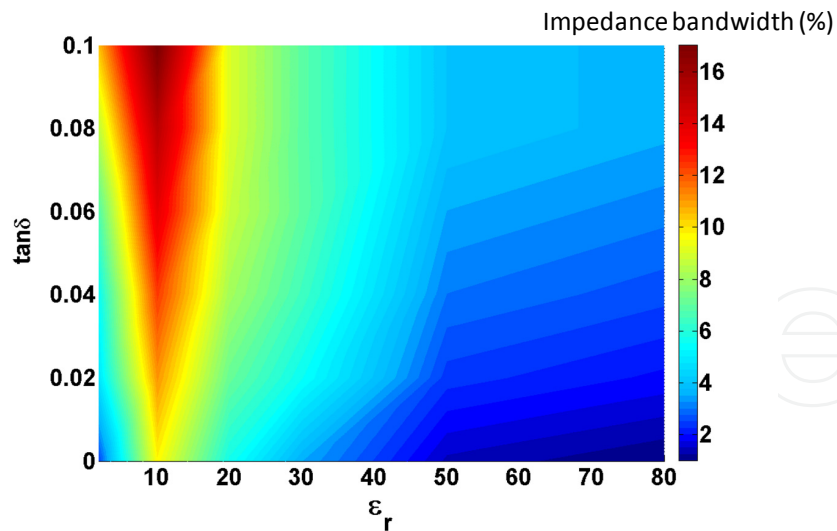


**Figure 14.** Impedance bandwidth according to the dielectric permittivity and loss tangent

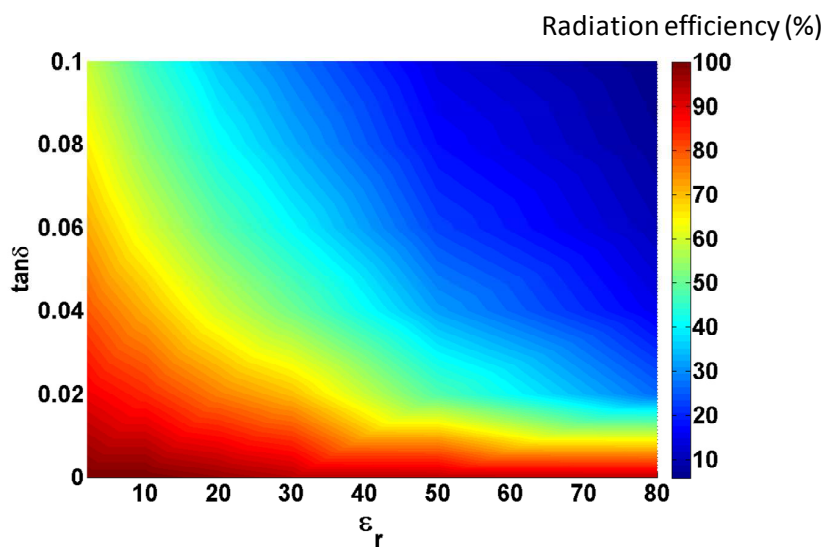


**Figure 15.** Radiation efficiency according to the dielectric permittivity and loss tangent

Other information can be deduced from this new graph:

- Antenna radiation efficiency is all the more affected by the losses as the dielectric permittivity increase.
- For low dielectric permittivity, even in case of a high losses material, the radiation efficiency remains higher than 50%.

To conclude this part, a DRA designer has to choose the dielectric material according to the application for which he is aiming. If he targets a wide bandwidth application, he could choose an alumina ceramic ( $\epsilon_r \sim 10$ ). Depending on the radiation efficiency he aims, the chosen ceramic would have more or less losses.

Now, if he targets an ultra-miniature DRA, it will be in his interest to choose a dielectric material with a higher dielectric permittivity. In this case, the impedance bandwidth will be affected, even more if the losses are high.



The dielectric material choice is one of the most important degree of freedom in the DRA design. It is necessary to highlight the best tradeoff, keeping in mind the targeted application.

Thus, using high dielectric permittivity values is one method for achieving a compact design, but it is not the only one. The next section will deal with different techniques to miniaturize a DRA.

#### 4. Overview of techniques to miniaturize DRAs

This part examines techniques to design compact DRAs. Targeted applications are mobile handsets or wireless tablet. There are several techniques to make DRAs more compact. By adding metal plates, inserting a high permittivity layer (multisegment DRA) or removing portions of the DRA, a significant size reduction can be achieved.

##### 4.1. Addition of a metallic plate on a DRA face

The rectangular DRA shape has been studied in the first part. The perfect metallic wall implies that electric fields are normal to this conductor, while magnetic fields are tangential. E and H fields presented Figure 11 assume that a metallic plate can be inserted in the middle of the DRA according to the y-component. The principle is detailed and explained by the Figure 16. It also shows the E and H fields of the  $TE_{111}$  mode.

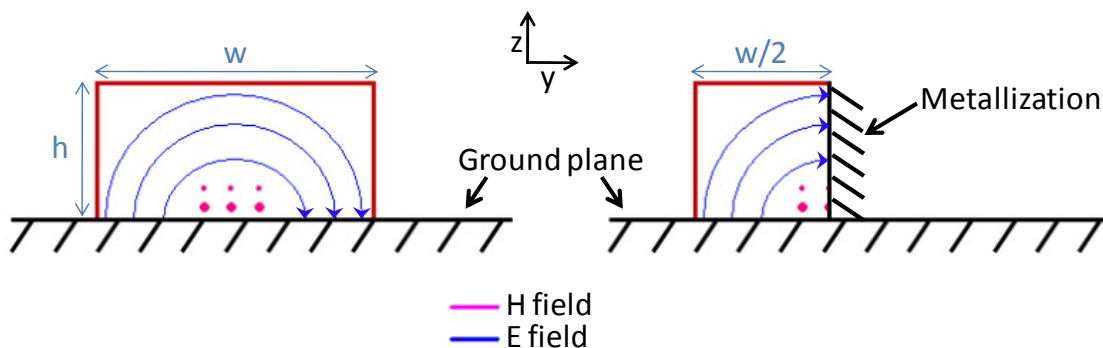


**Figure 16.** Integration of a metallic plate

By applying the image theory, it is possible to insert a metal plate in the  $y=w/2$  plane. The Table 1 extracted from [12] shows the influence of the metallic plate insertion on resonant frequency and impedance bandwidth.

$\epsilon_r$	w (cm)	d (cm)	h (cm)	Metallization	$f_0$ (GHz)	Bandwidth
12	2.75	2.75	2.95	No	1.98	10%
12	2.75	2.75	2.95	Yes	1.24	5.6%

**Table 1.** Influence of the metallic plate insertion on both resonant frequency and impedance bandwidth



Thus, the metal plate insertion allows dividing by two the DRA size, while reducing the resonant frequency. However, as pointed by the Table 1, the metallic plate insertion involves also the decrease of the impedance bandwidth.

## 4.2. Multisegment DRA

Another way to decrease the DRA size is to insert different substrate layers as illustrated Figure 17.

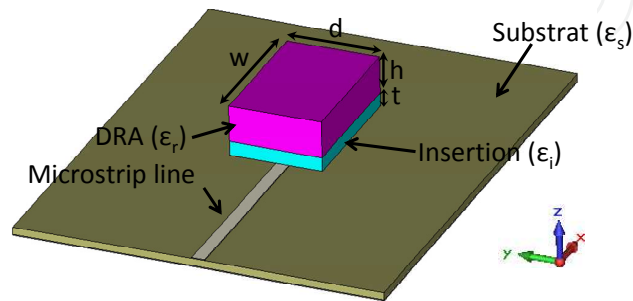


**Figure 17.** Multisegment DRA

It allows achieving strong coupling when the first insertion has a relatively high dielectric permittivity. This technique is detailed in [12] and [31]. The Table 2 summarizes a parametrical study done in [31] for one layer inserted (Figure 17) with  $w=7.875$  mm,  $d=2$  mm,  $h=3.175$  and  $\epsilon_r=10$ . It is mounted on a 0.762 mm height substrate of permittivity  $\epsilon_s=3$ . The  $TE_{111}$  mode of the DRA is excited with a  $50\Omega$  microstrip line.

t (mm)	$\epsilon_i$	Measured $f_0$ (GHz)	Bandwidth
0	-	15.2	21%
0.25	20	14.7	18%
0.635	20	14.5	18%
1	20	13.9	16%
0.25	40	14.7	20%
0.635	40	13.7	13%
1	40	12.9	5%
0.25	100	14.7	16%
0.635	100	13.1	7%
1	100	10.8	5%

**Table 2.** A parametrical study done in [31] for one layer inserted

Thus, a thin layer insertion allows improving the coupling of modes inside the DRA while decreasing the resonant frequency thanks to the decrease of the effective dielectric permittivity of the DRA. As the previous technique, the downside is the decrease of the impedance bandwidth.

### 4.3. Circular sector DRAs

To clearly explain this miniaturization technique, we need to take up the cylindrical DRA example with the equation 1 of the resonant frequencies. In [32], DRA size and resonance frequencies significant reductions have been demonstrated by using cylindrical sector DRA which is shown in Figure 18.

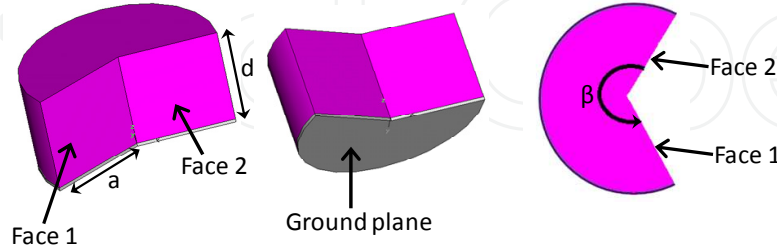


**Figure 18.** Circular sector DRA

As shows the Figure 18, a cylindrical sector DRA shape consists of a cylindrical DRA of radius  $a$  and height  $d$  mounted on a metallic ground plane, with a sector of dielectric material removed.  $\beta$  is the angle between the face 1 and 2, which can be metalized or left open. Thus, a cylindrical sector DRA is formed when  $\beta < 2\pi$ . For such a DRA, considering the equation 1, the  $n$  subscript can be substitute by the  $v$  subscript, which is a positive real number that depends on the boundary conditions on the sector faces as well as the sector angle  $\beta$ . In this case, first excited modes are writing such as  $HE_{v,pm+\delta^0}$  and the corresponding resonant frequencies as defined by the following equation:

$$f_{vpm} = \frac{c}{2\pi\sqrt{\epsilon_r\mu_r}} \sqrt{\left(\frac{X'_{vp}}{a}\right)^2 + \left(\frac{(2m+1)\pi}{2d}\right)^2} = \frac{c}{2\pi a\sqrt{\epsilon_r\mu_r}} \sqrt{\left(X'_{vp}\right)^2 + \left(\frac{(2m+1)\pi.a}{2d}\right)^2} \quad (7)$$

It should be noted that for the  $\beta = 2\pi$  case,  $v=n$ .

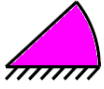


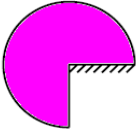
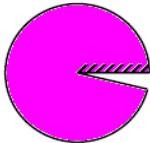
An important point has to be highlighted: For a given cylindrical sector DRA (radius, height, permittivity and permeability), the resonant frequency is only depending on the  $X'_{vp}$  value. The lower the  $X'_{vp}$  value will be, the lower the resonant frequency will be.  $X'_{vp}$  values are summarized in the Table 3.

	$v=0$	$v=1/4$	$v=1/3$	$v=1/2$	$v=2/3$	$v=1$	$v=2$
$p=1$	3.832	0.769	0.910	1.166	1.401	1.841	3.054
$p=2$	7.016	4.225	4.353	4.604	4.851	5.331	6.706

**Table 3.**  $X'_{vp}$  values according to the  $v$  and  $p$  values

By applying the good boundary conditions on each faces, fundamental modes of the different shapes presented in Table 4 can be determined. This table is reminding the  $X'_{vp}$  values with the corresponding resonant frequencies for a DRA such as  $a=40\text{mm}$  and  $d=45\text{mm}$  with a dielectric permittivity equals to 10.

Following these results, resonance frequencies depend on whether parts of some faces are coated with a metal or not. A good trade-off between antenna size and low resonant frequency is to choose the third line of the Table 4, when one face is coated by metal. Finally, this study has demonstrated that the metallization of some DRA faces allows creating new resonant modes, which have resonant frequencies lower than the fundamental modes inside a classical cylindrical DRA. It should be noted that these results have been done with cavity resonator model, i.e. the outer surfaces of the cavity are approximated by perfect magnetic walls. They thus show an approximate analysis of the fields inside the resonator. However, this model provides reasonable accuracy for prediction of resonant frequencies.

Mode	$\nu$	$p$	$X'_{\nu p}$	$f_{\nu pm}$	Shape
$HE_{21\delta}$	2	1	3.054	1.27 GHz	
$HE_{11\delta}$	1	1	1.841	872 MHz	
$HE_{1/2 1 \delta}$	1/2	1	1.166	687 MHz	
$HE_{1/3 1 \delta}$	1/3	1	0.910	629 MHz	
$HE_{1/4 1 \delta}$	1/4	1	0.769	602 MHz	

**Table 4.** Excited modes with the corresponding DRA shapes

## 5. New approaches for wireless applications

Antenna design for mobile communications is often problematic by the necessity to implement multiple and/or ultra wideband applications on the same small terminal.

Some of currently antennas integrated in portable wireless systems have a planar structure based on microstrip patches or PIFAs [33-35]. These kinds of antennas present a low efficiency, especially when small, because of metallic losses. DRAs do not suffer from such losses, which makes them a good alternative for these more conventional antennas. That is why, in recent years, much attention has been given to DRA miniaturization [16,36] in order to integrate them inside mobile handheld.

This part is divided in two sub-sections. The first one will focus on the bandwidth enhancement of a DRA for ultra wideband applications, and the second part will aim multiband applications. The common thread is the miniaturization of DRAs while obtaining good performances. For that, new hybrid modes will be studied with the application of partial electric boundary on sides of DRAs.

### 5.1. For ultra wideband application

A tendency and well known ultra wideband application is the Digital Video Broadcasting-Handheld (DVB-H). Indeed, the allocated frequency range is divided in two sub-bands, i.e. [470 MHz – 790 MHz] and [790 MHz – 862 MHz]. Considering the entire DVB-H frequency range, it presents 58% of bandwidth and a few kind of antenna can cover it instantaneously while being miniature and having good performances.

As presented in previous parts, for a single-mode excitation, the DRAs bandwidth doesn't exceed 15%. Recently, different shapes and stacked resonators have been proposed to enhance the bandwidth. These techniques are generally difficult to implement without increasing the size of the antenna. A novel DRA design method is proposed in this part with detailed parametric studies [37]. After seeing the proposed DRA and its miniaturization technique, the study will focus on the bandwidth enhancement. In order to design and optimize the proposed antenna, both eigenmode solver and the Finite Integration Temporal method of CST Microwave Studio are used. The measurement and simulation results will be shown, followed by a discussion.

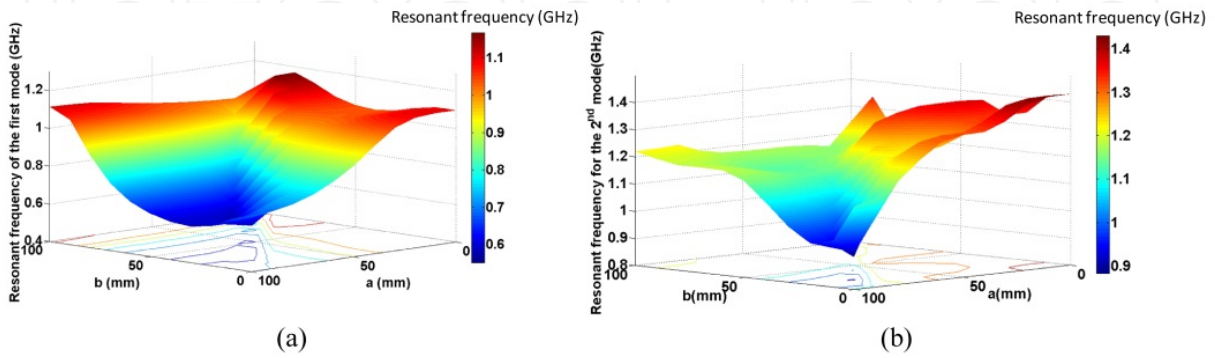
Previous parts have detailed the miniaturization technique by using a circular sector DRAs. It has been shown that resonance frequencies depend on whether parts of some faces are coated with a metal or not. According to the equation 7 and in order to easily integrate the antenna inside a terminal,  $d$  has to be lower than 25 mm. In this case, the lowest mathematical resonance frequency which can be obtained is 949MHz. The best compromise between the size and the desired frequency band is to use the  $HE_{\frac{1}{2},8}$  mode (Table 4). In order to entirely cover the DVB-H band, the non-coated face of the selected shape is transformed to a cubic part. The final designed DR shape is shown Figure 19.



**Figure 19.** Proposed DR shape (a) and metallization of two different sides (b)

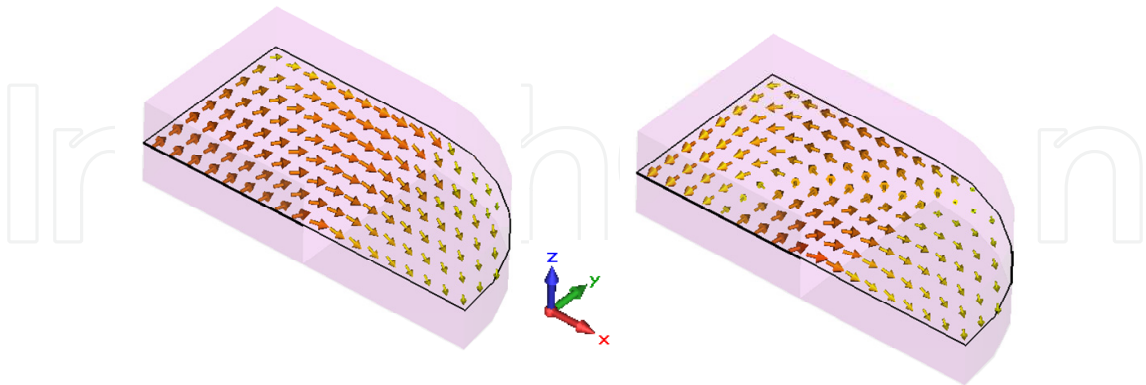
As mentioned previously, coating some faces with a metal allows resonance frequencies decreasing. A further parametric study is performed in order to determine how to coat some faces with a metal and how to choose the resonator position on the ground plane. In the Figure 19,  $a$  and  $b$  are defined as the metallization lengths of two different metallic sides.

Figure 20 represents the variation of the first and the second resonance frequencies mode according to  $a$  and  $b$  lengths.



**Figure 20.** Variation of the resonance frequency of the 1<sup>st</sup> (a) and 2<sup>nd</sup> (b) modes according to  $a$  and  $b$  lengths

The resonance frequencies decrease significantly when the two metallic sides have the same potential and each one covers half of the face. So, the optimum metallization lengths are  $a=50$ mm and  $b=50$ mm and the two lowest resonance frequencies are 568MHz and 1GHz. Through the above results, the chosen structure looks like the Figure 19 with  $a=b=50$ mm. Now, it is necessary first of all to glance over the E-field distribution inside the DR. Figure 21 shows the E-field inside the DR for the first and the second mode respectively at 568 MHz and 1 GHz. The first mode is derivative from the  $HE_{\frac{1}{2}18}$  mode.



**Figure 21.** E fields of the two first modes

In the following, a ground plane is inserted on the lower metallic face as shown Figure 22. The ground plane size is 230mm x 130mm, chosen to correspond to a standard DVB-H handheld receiver. The DR of  $\lambda_0/7 \times \lambda_0/13 \times \lambda_0/28$  dimensions at 470 MHz is mounted on such ground plane.

Considering the E fields distribution, a probe is chosen to feed the DRA. It is placed on the lateral metallic side in order to simultaneously excite the two first modes (Figure 22).

To reach an ultra wideband, the probe position, diameter and length are tuned. The optimal probe diameter and length values are 1.5mm and 49mm.

Following this optimization, input impedance and return loss are shown in the Figure 23.

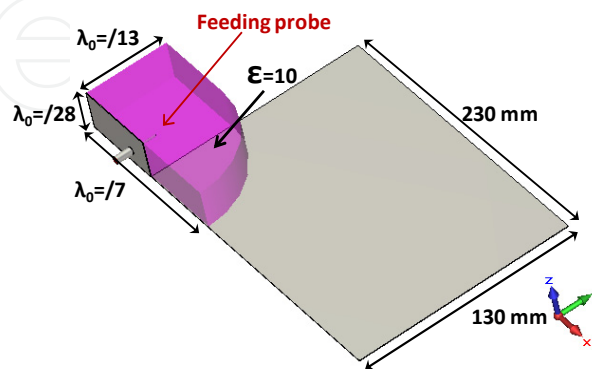


**Figure 22.** Antenna design fed by a coaxial probe

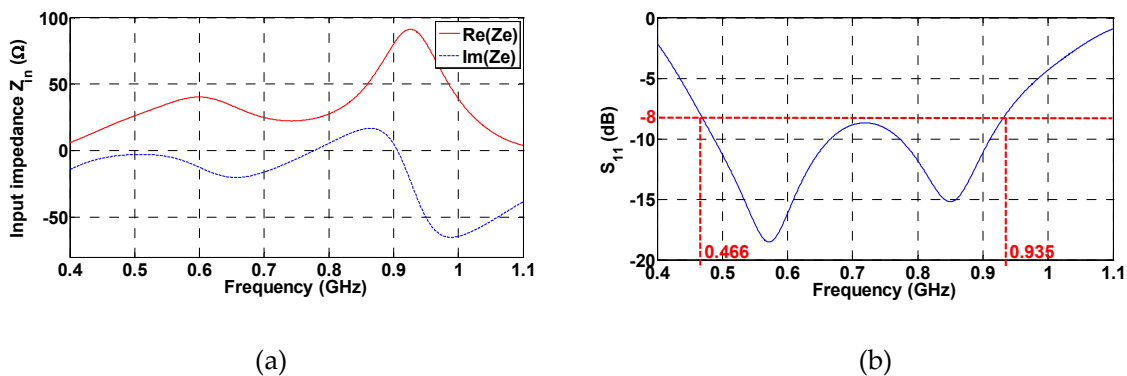


**Figure 23.** Input impedance (a) and  $S_{11}$  parameter (b) of the considered DRA

They show that two modes exist at 0.6 MHz and 0.93 MHz, excited by the coaxial probe. As expected, a difference appears between resonance frequency values which are obtained by the eigenmode solver and electromagnetic simulation. This discrepancy is due to the presence of the probe and the ground plane. Furthermore, the boundary conditions applied during the modal analysis are perfect electric or magnetic conditions on the DR walls contrarily to the electromagnetic simulation.

The simulated coefficient reflection shows 70% of bandwidth for a -8 dB impedance bandwidth definition over the frequency range [466 MHz – 935 MHz]. The -8dB impedance bandwidth definition is sufficient to achieve a good efficiency. Thus, the antenna satisfies the DVB-H system specifications mentioned previously. To demonstrate the antenna performances, the antenna has been realized with a ceramic material. It is fed by a probe and is half-mounted on a ground plane. The manufactured antenna is shown Figure 24.



The input impedance and the coefficient reflection are shown Figure 25.

There is a good agreement between simulations and measurements. It should be underlined that these simulations series take into account that the probe is inserted in a 2 mm diameter hole instead of a 1.5 mm hole due to mechanical constraint, therefore an air gap appears around the probe. This air gap results in lowering the DRA effective dielectric constant, which is turn lower the Q-factor accompanied by a shift in the resonance frequency. Furthermore, after material characterizations, the ceramic's dielectric constant turns out equal to 9.5 at 500 MHz. So, the -8dB impedance matching bandwidth is included in [540 MHz – 1.05 GHz].

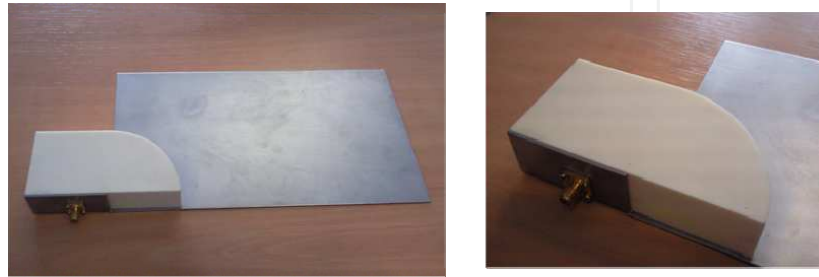


**Figure 24.** Antenna prototype

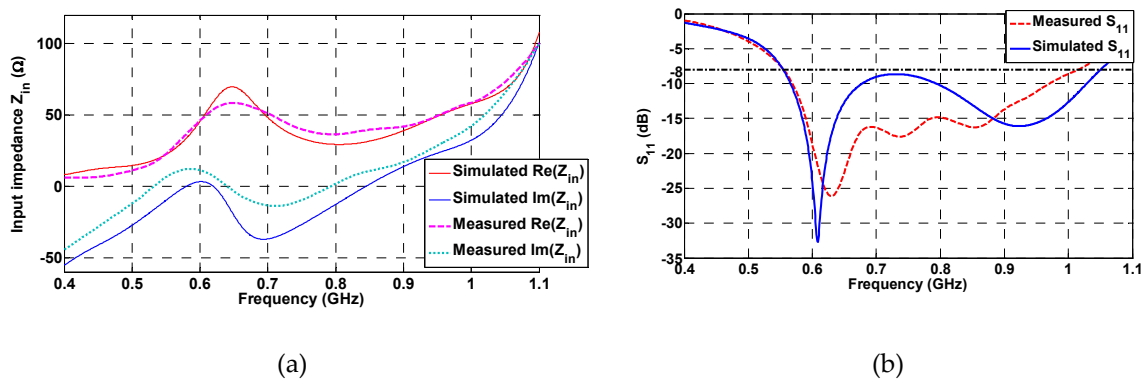


**Figure 25.** Measured and simulated input impedances (a) and  $S_{11}$  parameters (b)

Radiation patterns of the antenna were characterized in an anechoic chamber. Simulated and measured radiation patterns at 620MHz and 870MHz are shown Table 5.

It can be noticed that the  $xz$ -plane and  $yz$ -plane radiation patterns indicate a correct omnidirectional radiation patterns. The antenna operates at two different modes inside the operating band, so the antenna doesn't offer the same radiation pattern at the two resonance frequencies, particularly in the  $xy$ -plane. The simulated and measured total efficiencies of the proposed antenna are illustrated Figure 26.

This efficiency disagreement is probably due to the coaxial feeding cable, the discrepancy between the simulated and measured reflection coefficient and the dielectric loss tangent.

In spite of this 10% difference, there is a good agreement between measured and simulated efficiencies. The measured efficiency remains higher than 75% above 600MHz.



This part has proposed a novel dielectric resonator antenna. Parametric studies have been realized to decrease resonance frequencies and to increase impedance matching bandwidth. The results have shown that by shaping the dielectric structure and coating some faces with a metal, resonance frequencies have been reduced for a fixed structure size. Good performances have been obtained and the proposed antenna can be used for DVB-H and/or GSM900 applications with a wide bandwidth and a good efficiency.

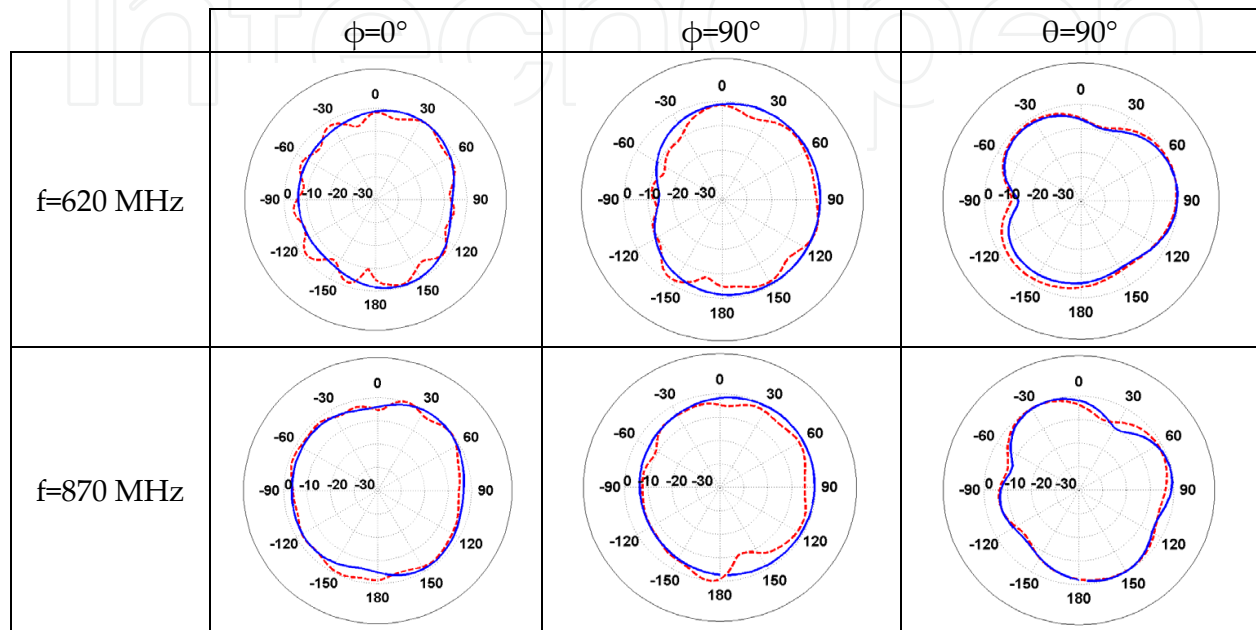


**Table 5.** Simulated (blue line) and measured (red line) radiation patterns at 620 MHz and 870 MHz

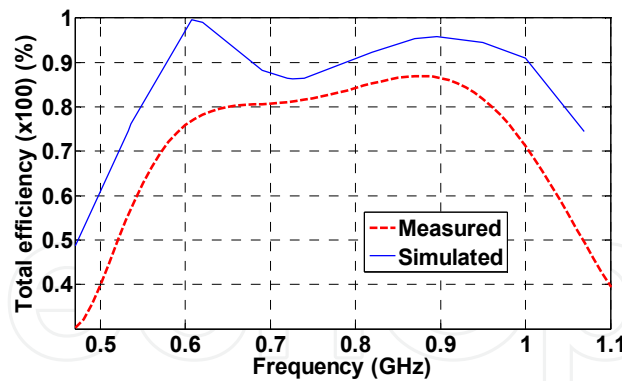


**Figure 26.** Measured and simulated total efficiencies of the considered DRA

### 5.2. For multiband application

In the last decade, the huge demand for mobile and portable communication systems has led to an increased need for more compact antenna designs. This aspect is even more critical when several wireless technologies have to be integrated on the same mobile wireless communicator. All the new services and the increased user density are driving the antenna design toward multi-band operation.

Recently, many studies have been devoted to multi-band antennas [38-41], some of them dealing with DRAs [42-44]. A dielectric resonator indeed supports more than one resonant mode at two close frequencies, which allows them to meet the requirements of different applications with a unique device. Some studies furthermore use both the dielectric resonator and the feeding mechanism as radiator elements [43-45]. This explains why the DRAs present a major advantage for multi-standard devices, when compared to other kinds of antennas.

The objective of this part is to show the integration of a small antenna in a multi-band mobile handheld device, working on the nine channels of the second sub-band of the DVB-H, i.e. [790 MHz – 862 MHz], the WiFi band at 2.4 GHz and the WiMax band at 3.5 GHz. Additionally, in order to improve the quality and the reliability of the wireless links, i.e. obtain pattern diversity, two antennas will be integrated in the same device. Setting maximum limits, we have decided to integrate two orthogonally aligned antennas in the allocated space of 30 mm x 41 mm ( $\lambda_0/13 \times \lambda_0/9$  at 800 MHz), on a 230 mm x 130 mm ground plane. Each DRA will therefore have to be very compact to be able to fit in such a limited area, and will operate around 850 MHz, 2.4 GHz and 3.5 GHz, thus covering the nine channels of the DVB-H band, the WiMax and the WiFi band.

Firstly, only one radiating element is described. It will be done thanks to a modal analysis [46] of the dielectric resonator. The DRA design and the choice of the dielectric permittivity will be discussed. As for the previous sub-section, both the Finite Integration Temporal method and the eigenmode solver of CST Microwave Studio were used to carry out this work.

Getting three resonant frequencies for a single dielectric resonator is aiming. Firstly, the resonator has to be integrated in a handheld receiver, which means that it will be placed on a FR4 substrate ( $\epsilon_r=4.9$ ). Secondly, to be integrated in a handheld device, the allocated space for the antenna system must not exceed 41mm x 30 mm x 4mm as shown Figure 27.

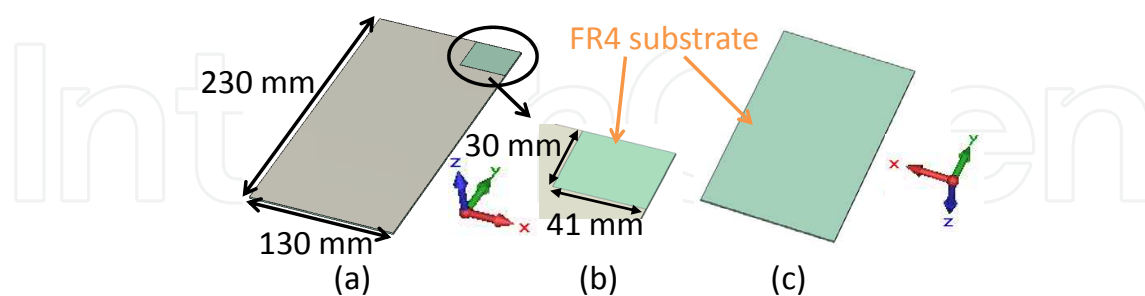


**Figure 27.** Top view of the defined PCB card (a), allocated size for the antenna system (b) and bottom view of the defined PCB card (c)

The dimensions and dielectric permittivity of each resonator need to be chosen according to these constraints, to ensure the integration of the antenna in the final device.

As a result, the dimensions of one resonator were chosen to be 25 mm x 10 mm x 4 mm, with a very high dielectric constant  $\epsilon_r$  of 37. The resulting geometry is depicted Figure 28.

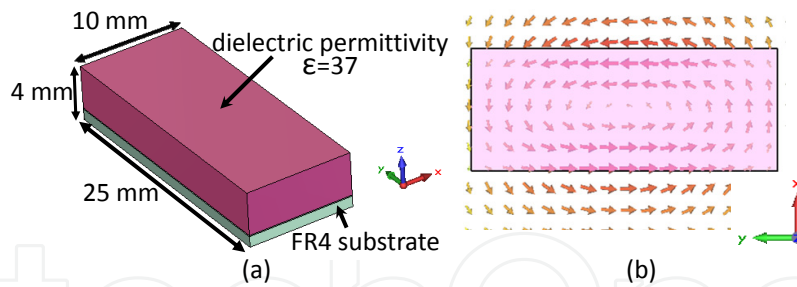


**Figure 28.** Dimensions and properties of one resonator (a) and E-field distribution of the first natural mode for the resonator in (b) in the  $z=2\text{mm}$  plane

The first natural mode of this resonator is the  $TE_{11\delta}$  (Figure 28) which resonates at 3.99 GHz. This resonance frequency remains too high for the intended applications. It has however been shown [37], that this resonance frequency depends on the metallization of the DRA's faces. It is therefore necessary to envision the feeding mechanism of the resonator, before performing the modal analysis. Indeed, if the antenna is not fed by proximity coupling, the excitation cannot be ignored during the modal analysis. Furthermore, it can be used to adjust the resonance frequency of the resonator, especially in the case of an electrically small DRA. In this study, the feeding will indeed play a preeminent role. The chosen excitation is a line printed on the FR4 substrate and positioned under the dielectric resonator as shown Figure 29. The E-field distribution of the first mode (Figure 29) is completely different from the one obtained without this line. Indeed, as stated before, the E-field and H-field distributions inside the DRA depend on the boundary conditions on its faces. The feeding line introduces partially perfect electric conducting conditions, which disturb the field distribution inside the resonator when compared with the  $TE_{11\delta}$  mode. As a result, the resonance frequency of each mode will vary in accordance with the length and width of the feeding line (defined in the Figure 29).

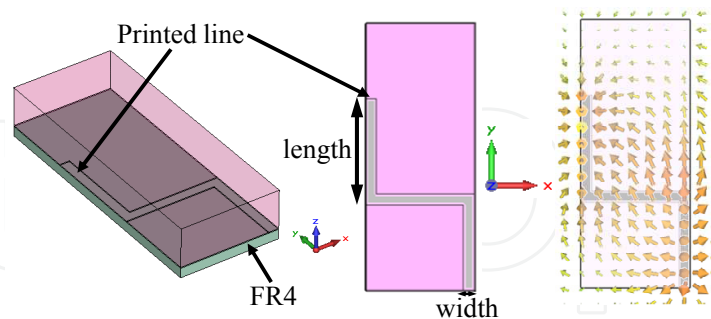


**Figure 29.** Design of the DRA fed by the printed line and E-field distribution of the first natural mode for the resonator fed by the line

Considering the previous study, the resonator design method is as follows.

- First of all, in spite of the high dielectric permittivity, there is no mode around 800 MHz. In order to allow the antenna to operate on the nine channels of the DVB-H band, the printed line will be designed to resonate around 800 MHz. It will therefore behave like a printed monopole loaded by a dielectric. The length of this line, which will from

now be referred as the “monopole”, will be set to obtain the first resonance frequency around 800 MHz.

- This being done, the second and third band will be covered by the resonances of the dielectric resonator disturbed by the presence of the monopole. As previously explained, the length, width and shape of this monopole entail a modification of the DRA resonance frequencies. The shape and width of the monopole will therefore be optimized to obtain the desired resonance frequencies, while its length remains set by the first resonance.
- An important point concerns the radiation Q-factor. The high dielectric permittivity involves a high Q-factor [7]. With such an  $\epsilon_r$ , the radiation Q-factor is also important, making it difficult to obtain a wide impedance bandwidth for a given mode. So, to have a suitable impedance bandwidth, the antenna will have to be matched between two peaks of the real part of input impedance. By this way, the resonances won't have to be close to the operating bands. The goal being to match the DRA over the WiFi and WiMax bands, the monopole (its shape and width) has to be optimized to obtain resonance frequencies around 2 GHz, 2.8 GHz and 4 GHz.
- A modal analysis has been performed to show the variations of the resonance frequencies of the first three modes, according to the shape and width of the monopole. Figure 30 shows the resonance frequency of the first mode according to the monopole geometry. With the first resonance frequency set to match the antenna at 2.4 GHz and the length of the monopole set to have the first resonance at 800 MHz, the graph of the modal analysis allows an easy determination of the monopole width, which is 1 mm.

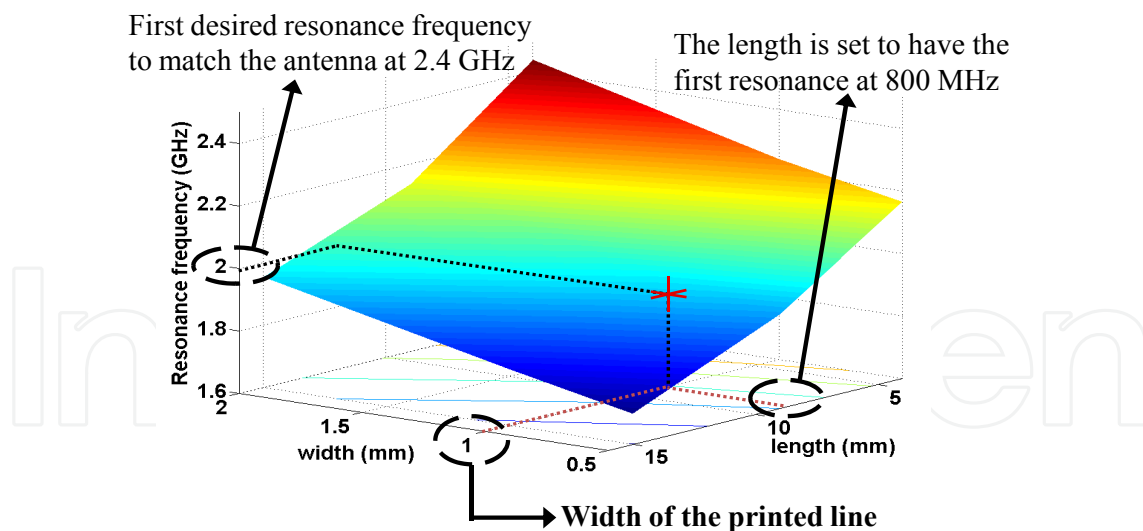


**Figure 30.** : Resonance frequency of the first dielectric resonator mode according to the width and the length of the monopole previously defined

Same studies have been performed for different shapes of the monopole. All these studies allowed the shape, length and width of the monopole to be set, which led to the final design of the dielectric resonator. Table 6 shows the values of the resonance frequencies for the first three modes inside the resonator, which were obtained through the modal analysis.

Mode	Resonance frequency
First mode	1.969 GHz
Second mode	2.773 GHz
Third mode	4.135 GHz

**Table 6.** Values of Resonance Frequency for the Three First Modes

- Electromagnetic study of the DRA

In order to validate the previous modal study, the dielectric resonator, placed in the area dedicated to the antenna (Figure 27) and fed by a 50 $\Omega$  discrete port, has been simulated with the FIT method using CST Microwave Studio. It must be noticed that a discrete port is modeled by a lumped element, consisting of a current source with a 50  $\Omega$  inner impedance that excites and absorbs power.

The Figure 31 shows the simulated input impedance of the dielectric resonator with its feed. The resonance frequencies are in agreement with the modal analysis. The radiation Q-factor is important, and the input impedance variations confirm that the antenna matching is easier between two resonances. The reflection coefficient is shown Figure 31. The antenna is matched on all of the desired bands, i.e. the nine channels of DVB-H going from 790 MHz to 862 MHz, the WiFi band at 2.4 GHz and the WiMax band at 3.5 GHz. It can be noted that the matching over the first band is obtained due to the resonance of the  $\lambda/4$  monopole.

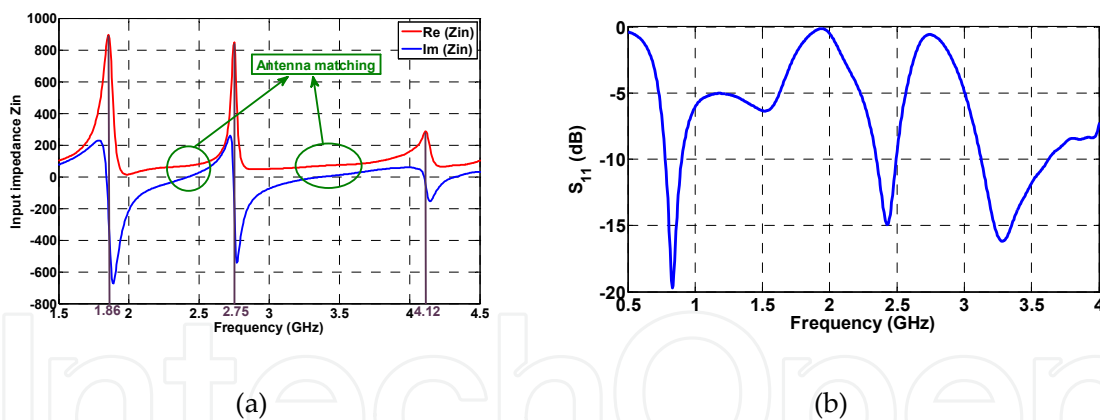


**Figure 31.** Input impedance (a) and  $S_{11}$  parameter of the fed DRA

The dielectric resonator must now be integrated in its context, i. e. on a 230 mm  $\times$  130 mm ground plane, chosen to correspond to a standard DVB-H handheld receiver. As explained before, another specification was to obtain a reconfigurable radiation pattern. Thus, two instances of the previously studied resonator are orthogonally integrated on the ground plane.

- Final structure

Based on the previous parametric study, the final structure has been designed as shown Figure 32. In order to obtain pattern diversity, two dielectric resonators are orthogonally

disposed in a 30 mm x 41 mm area, both fed by a printed line acting as a monopole. Each line is fed by a 50Ω coaxial cable. They are studied on a 230 mm x 130 mm ground plane, as defined by the specifications. It will be shown in a following section that the antenna matching is not affected by the ground plane dimensions. In order to ascertain the performances of this antenna, a prototype has been fabricated as shown Figure 32.

The resonators are manufactured with a ceramic material with a dielectric permittivity of 37 and a loss tangent  $\tan\delta=0.005$  on the 0.5-10 GHz band. During the simulation and measurements, each resonator has been excited by a printed line fed by a coaxial cable.

During the manufacturing process of the antenna, a special care has to be given to minimize the air gap between the excitation and the resonator. In the case of this prototype, the resonators have been pressed onto the PCB to avoid this air gap.

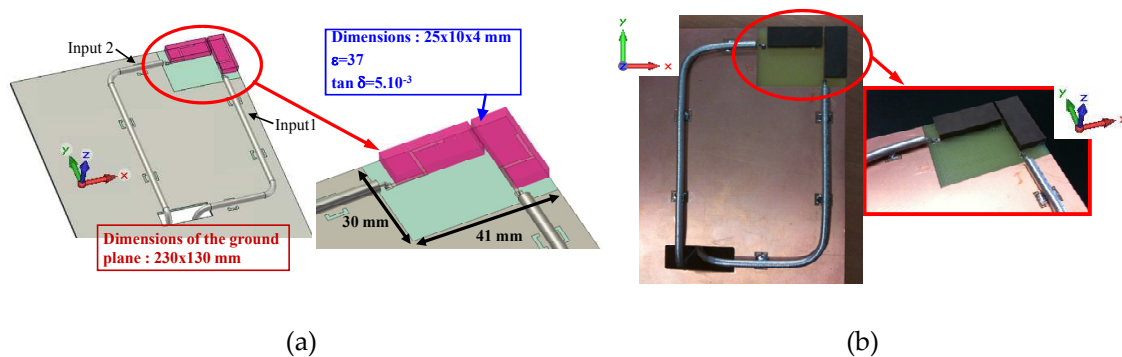


**Figure 32.** Final simulated design (a) and the corresponding prototype (b)

- Measured and simulated performances of the antenna

The comparison between the simulated and measured results is now studied. The first ones have been obtained using the transient solver of CST Microwave Studio, while the measurements have been performed inside an anechoic chamber. Both the simulated  $S_{11}$  and  $S_{22}$  parameters are compared with the measured ones Figure 33.

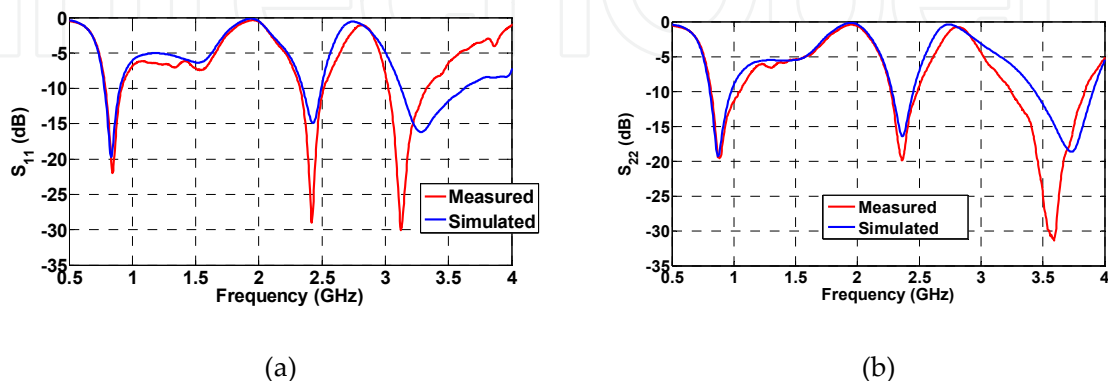


**Figure 33.** Measured and simulated  $S_{11}$  (a) and  $S_{22}$  (b) parameters of the DRA



The measurements and simulations are in very good agreement. Moreover, the antenna is matched over all the desired bands and for both inputs.

Radiation patterns: The radiation patterns have been measured inside an anechoic chamber. Table 7 shows the 3D simulated radiation patterns for both inputs at 830 MHz, 2.4 GHz and 3.5 GHz.

It can be seen that the radiation pattern at a given frequency will depend on the excited port. While promising, this result is not sufficient to conclude that the radiation pattern is reconfigured. More details are explained in [47] (this requires the characterization of the whole system in a reverberation chamber, in order to determine the correlation coefficient).

Thus, this study started with modal analyses, which allowed the shape and dimensions of the antenna's excitation to be defined with a dual objective. Indeed, this line had first to behave like a monopole and cover the nine channels of the DVB-H band (going from 790 MHz to 862 MHz). Secondly, it had to excite the dielectric resonator and set its resonance frequencies so as to match the antenna on the WiFi and WiMax bands.

After performing these preliminary studies, two instances of the conceived dielectric resonator have been orthogonally integrated on a 230 mm x 130 mm ground plane, which is consistent with a tablet. Finally, the antenna system, which only occupies a 30 mm x 41 mm area, is matched on the three desired bands, i.e. the nine channels of the DVB-H band, the WiFi band and the WiMax band with pattern diversity.

This part has presented the design method, the realization and the measurement of a two compact DRAs, one for ultra wideband application and the second for multiband applications.

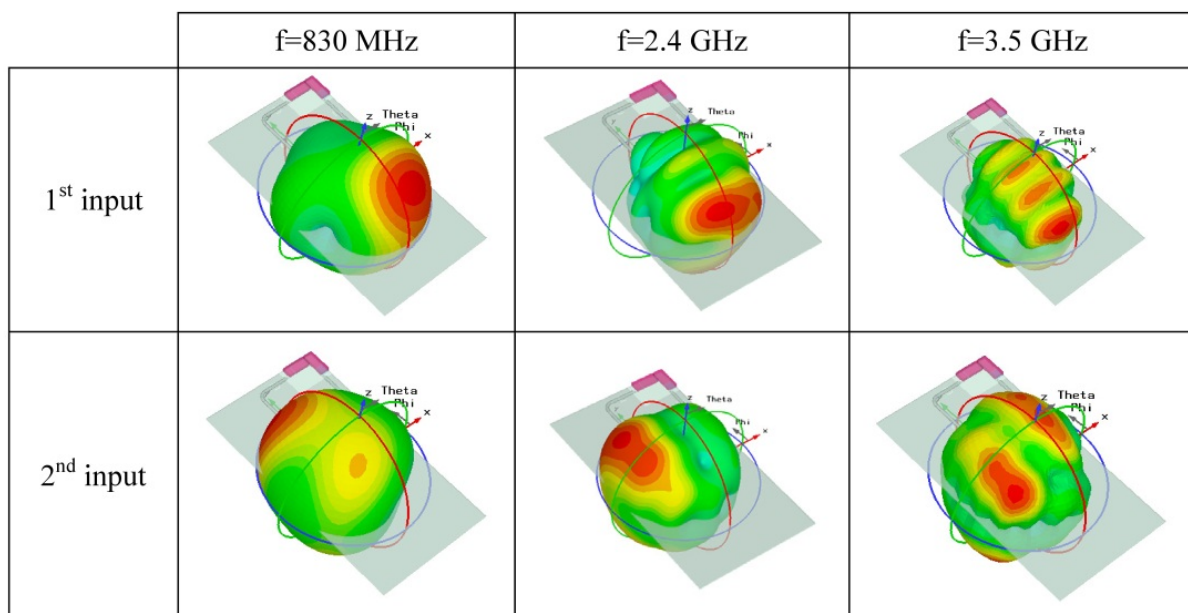


**Table 7.** 3D Radiation patterns at 830 MHz, 2.4 GHz and 3.5 GHz for the two inputs



## 6. Conclusion

To conclude, an affordable chapter has been presented allowing the reader to find an overview of main DRA shapes, properties and approaches while appreciating the influence and the impact of the dielectric material properties. Indeed, a broad spectrum of dielectric materials can be used depending on the intended application. In addition to the advantages common to all DRAs described at the beginning of this chapter, a dedicated part has focused on other advantages of compact DRAs, which are desirable for many emerging wireless and mobile communication systems. Finally, a specific part had presented relevant data for postgraduate researchers, antenna design engineers in general and particularly the ones engaged in the innovative design of mobile and wireless systems by focusing on the hybrid modes creation to enhance the bandwidth or develop multiband antennas.

## Author details

L. Huitema and T. Monediere

*University of Limoges, Xlim Laboratory, France*

## 7. References

- [1] R. D. Richtmyer, "Dielectric Resonator", J. Appl. Phys., vol. 10, pp. 391-398, Jun. 1939
- [2] D. Kajfez and P. Guillon, Eds., Dielectric Resonators. Norwood, MA: Artech House, 1986
- [3] Cohn, S.B., "Microwave Bandpass Filters Containing High-Q Dielectric Resonators," Microwave Theory and Techniques, IEEE Transactions on, vol.16, no.4, pp. 218- 227, Apr 1968
- [4] S. J. Fiedziuszko, "Microwave Dielectric Resonators", Microwave Journal, vol. 29, September 1986, pp 189-200
- [5] S.A. Long, M.W. McAllister and L.C. Shen, "The Resonant Dielectric Cavity Antenna", IEEE Transactions on Antennas and Propagation, Vol. 31, n°3, March 1983, pp. 406-412
- [6] A. Petosa, A. Ittipiboon, Y.M.M. Antar and D. Roscoe, "Recent Advances in Dielectric Resonator Antenna Technology", IEEE Antennas and Propagation Magazine, Vol. 40, n°3, 06/1998, pp. 35-48
- [7] K.M Luk and K.W Leung, "Dielectric Resonator Antennas", Electronic & Electrical Engineering Research Studies
- [8] R.K Mongia and A. Ittipiboon, "Theoretical And Experimental Investigations on Rectangular Dielectric Resonator Antenna", IEEE Transactions on Antennas and Propagation, Vol. 45, n°9, September 1997, pp. 1348-1356
- [9] D. Drossos, Z. Wu and L.E. Davis, "Theoretical and experimental investigation of cylindrical Dielectric Resonator Antennas", Microwave and Optical Technology Letters, Vol. 13, No. 3, pp. 119-123, October 1996
- [10] R. K. Mongia and P. Bhartia, "Dielectric Resonator Antennas – A review and General Design Relations for resonant Frequency and Bandwidth", International Journal of

- Microwave and Millimeter-wave Computer-Aided Engineering, Vol. 4, No. 3, pp. 230-247, Mar. 1994
- [11] A.A. Kishk, B. Ahn and D. Kajfez, "Broadband stacked dielectric resonator antennas", IEE Electronics Letters, Vol. 25, n°18, Aug. 1989, pp. 1232-1233
- [12] A. Petosa, "Dielectric Resonator Antenna Handbook", Artech House, Boston/London, 2007
- [13] R. Chair, A. A. Kishk, K. F. Lee, "Wideband Stair-Shaped Dielectric Resonator Antennas," IET Microwaves, Antennas & Propagation, Vol. 1, Issue 2, pp. 299-305, April 2007
- [14] Wei Huang and Ahmed Kishk, "Compact Wideband Multi-Layer Cylindrical Dielectric Resonator Antenna," IET Microwave Antenna and Propagation, Vol. 1, no. 5, pp. 998-1005, October 2007
- [15] R. Chair, A. A. Kishk, K. F. Lee, "Low Profile Wideband Embedded Dielectric Resonator Antenna," IET Microwaves, Antennas & Propagation, Vol. 1, Issue 2, pp. 294 - 298, April 2007
- [16] Y. Gao, B. L. Ooi, W. B. Ewe, A. P. Popov, "A compact wideband hybrid dielectric resonator antenna", IEEE Microw.Wirel. Compon. Lett., 2006, 16, (4), pp. 227-229
- [17] K. A. A. Wei Huang, "Use of electric and magnetic conductors to reduce the DRA size", Int. Workshop on Antenna Technology: Small and Smart Antennas Metamaterials and Applications, IWAT '07, 2007
- [18] J.M Ide, S.P Kingsley, S.G O'Keefe, S.A Saario, "A novel wide band antenna for WLAN applications," Antennas and Propagation Society International Symposium, 2005 IEEE , vol.4A, no., pp. 243- 246 vol. 4A, 3-8 July 2005
- [19] L. Huitema, M. Koubeissi, C. Decroze, T. Monediere, "Handheld Dielectric Resonator Antenna for Ultra Wideband Applications", 2010 IEEE International Workshop on Antenna Technology: iWAT2010: « Small Antennas and Novel Metamaterials» March 1-3, 2010, pp. 1-4, Portugal
- [20] L. Huitema, M. Koubeissi, C. Decroze, T. Monediere, "Compact and multiband dielectric resonator antenna with reconfigurable radiation pattern," Antennas and Propagation (EuCAP), 2010 Proceedings of the Fourth European Conference on , vol., no., pp.1-4, 12-16 April 2010
- [21] A. Sangiovanni, J. Y. Dauvignac and Ch. Pichot, "Stacked dielectric resonator antenna for multifrequency operation", Microw. and Opt. Techn. Lett., vol. 18, pp. 303-306, July 1998
- [22] Z. Fan and Y.M.M. Antar, "Slot-Coupled DR Antenna for Dual-Frequency Operation," IEEE Trans. Antennas and Propagation, Vol. 45, No. 2, Feb. 97, pp. 306-308
- [23] G.P. Junker, A.A. Kishk, A.W. Glisson and D. Kajfez, "Effect of an air gap around the coaxial probe exciting a cylindrical dielectric resonator antennas", Electronics Letters, Vol. 30, No. 3, pp. 177-178, 3<sup>rd</sup> February 1994
- [24] G.P. Junker, A.A. Kishk, A.W. Glisson and D. Kajfez, "Effect of air gap on cylindrical dielectric resonator antennas operating in TM<sub>01</sub> mode", Electronics Letters, Vol. 30, No. 2, pp. 97-98, 20<sup>th</sup> January 1994

- [25] Kwok-Wa Leung; Kwai-Man Luk; Lai, K.Y.A.; Deyun Lin; , "Theory and experiment of an aperture-coupled hemispherical dielectric resonator antenna," *Antennas and Propagation, IEEE Transactions on* , vol.43, no.11, pp.1192-1198, Nov 1995
- [26] A.A. KISHK, A. ITTIPIBOON, Y. ANANTAR, M. CUHACI "Slot Excitation of the dielectric disk radiator", *IEEE Transactions on Antennas and propagation*, vol. 43, N°2, pp.198-201, Feb 1993
- [27] A.W. Glisson, D. Kajfez and J. James, "Evaluation of modes in dielectric resonators using a surface integral equation formulation," *IEEE Trans. Microwave Theory Tech.*, Vol. MTT-31, pp. 1023-1029, 1983
- [28] D. Kajfez, A. W. Glisson and J. James, "Computed modal field distributions for isolated dielectric resonators," *IEEE Trans. Microwave Theory Tech.*, Vol.MTT-32, pp. 1609-1616, 1984
- [29] Y. Kobayashi and S. Tanaka, "Resonant Modes of a dielectric rod resonator short circuited at both ends by parallel conducting plates", *IEEE Trans. Microwave Theory and Tech.*, Vol. 28, pp. 1077-1085, Oct. 1980
- [30] Van Bladel, J., "On the Resonances of a Dielectric Resonator of Very High Permittivity," *Microwave Theory and Techniques, IEEE Transactions on* , vol.23, no.2, pp. 199- 208, Feb 1975
- [31] Petosa, A.; Simons, N.; Siushansian, R.; Ittipiboon, A.; Cuhaci, M.; , "Design and analysis of multisegment dielectric resonator antennas ," *Antennas and Propagation, IEEE Transactions on* , vol.48, no.5, pp.738-742, May 2000
- [32] M.T.K Tam and R.D Murch, "Compact circular sector and annular sector dielectric resonator antennas", *IEEE Transactions on antennas and Propagation*, Vol. 47, n° 5, 1999, pp. 837-842
- [33] C. W. Ling, C. Y. Lee, C. Y. Tang, and S. J. Chung "Analysis and Application of an On-Package Planar Inverted-F Antenna", *IEEE Transactions on Antennas and Propagation*, Vol. 55, n°6, June 2007, pp. 1774 - 1780.
- [34] M. J. Ammann and L. E. Doyle, "A loaded inverted-F antenna for mobile handset," *Microwave Opt. Technol. Lett.*, vol. 28, pp. 226–228, 2001.
- [35] M. Ali and G. J. Hayes, "Analysis of integrated inverted-F antennas for Bluetooth application," in *Proc. IEEE-APS Conf. Antennas and Propagation for Wireless Communications*, Waltham, MA, 2000, pp. 21–24.
- [36] K. A. A. Wei Huang, "Use of electric and magnetic conductors to reduce the DRA size", *Int. Workshop on Antenna Technology: Small and Smart Antennas Metamaterials and Applications, IWAT '07*, 2007
- [37] L. Huitema, M. Koubeissi, C. Decroze, T. Monediere, "Ultrawideband Dielectric Resonator Antenna for DVB-H and GSM Applications" *IEEE Antennas and Wireless Propagation letter*, vol. 8, pp. 1021-1027, 2009
- [38] Y.-Y. Wang and S.-J. Chung, "A new dual-band antenna for WLAN applications," in *Proc. IEEE AP-S Int. Symp.*, Jun. 20–25, 2004, vol. 3, pp. 2611–2614.
- [39] Jan, J. Y. and L. C. Tseng, "Small planar monopole antenna with a shorted parasitic inverted-L wire for wireless communications in the 2.4-, 5.2-, and 5.8-GHz bands," *IEEE Trans. Antennas Propag.*, Vol. 52, 1903-1905, 2004

- [40] Z. D. Liu and P. S. Hall, "Dual-band antenna for handheld portable telephones," *Electron. Lett.*, vol. 32, pp. 609–610, 1996.
- [41] J. Y. Jan and L. C. Tseng, "Planar monopole antennas for 2.4/5.2 GHz dual-band application," in *Proc. IEEE-APS Int. Symp. Dig.*, Columbus, OH, 2003, pp. 158–161
- [42] K. Hady, A. A. Kishk and D. Kajfez, "Dual-Band Compact DRA With Circular and Monopole-Like Linear Polarizations as a Concept for GPS and WLAN Applications", *IEEE Trans. on ant. and propog.*, Vol. 57, No. 9, 2591-2598, September 2009.
- [43] Rao, Q.; Denidni, T.A.; Sebak, A.R.; Johnston, R.H.; , "Compact Independent Dual-Band Hybrid Resonator Antenna With Multifunctional Beams," *Antennas and Wireless Propagation Letters, IEEE* , vol.5, no.1, pp.239-242, Dec. 2006
- [44] Rotaru, M.; Sykulski, J.K.; , "Numerical investigation on compact multimode dielectric resonator antennas of very high permittivity," *Science, Measurement & Technology, IET* , vol.3, no.3, pp.217-228, May 2009
- [45] Qinjiang Rao; Denidni, T.A.; Sebak, A.R.; , "A hybrid resonator antenna suitable for wireless communication applications at 1.9 and 2.45 GHz," *Antennas and Wireless Propagation Letters, IEEE* , vol.4, no., pp. 341- 343, 2005
- [46] R.A Kranenburg, S.A Long, "Microstrip transmission line excitation of dielectric resonator antennas," *Electronics Letters* , vol.24, no.18, pp.1156-1157, 1 Sep 1988
- [47] L. Huitema, M. Koubeissi, M. Mouhamadou, E. Arnaud, C. Decroze And T. Monediere, "Compact and Multiband Dielectric Resonator Antenna with Pattern Diversity for Multi Standard Mobile Handheld Devices", *IEEE Transaction on antennas and propagation*, vol. 59, pp.4201-4208, 2011